Supporting information

Targeted therapy of atherosclerosis by zeolitic imidazolate framework-8 nanoparticles loaded with losartan potassium via simultaneous lipid-scavenging and anti-inflammation

Jie Sheng[†a], Ziyue Zu[†a], Yugang Zhang[†b], Haitao Zhu[†c], Jianchen Qi[a], Tao Zheng[a], Ying Tian[a], Longjiang Zhang[*a]

1. *Department of Radiology, Jinling Hospital, School of Medicine, Nanjing University, Nanjing 210002, China*
2. *State Key Laboratory of Radiation Medicine and Protection,School for Radiologica and Interdisciplinary Sciences (RAD-X) and Collaborative Innovation Center of Radiation Medicine of Jiangsu Higher Education Institutions, Soochow University, Suzhou 215123, China*
3. *Affiliated Hospital of Jiangsu University, Jiangsu University, Zhenjiang, 212001, China,*

Keywords: zeolitic imidazolate framework-8 (ZIF-8), autophagy, atherosclerosis, losartan potassium (LP), drug delivery, reverse cholesterol transport (RCT), anti-inflammatory

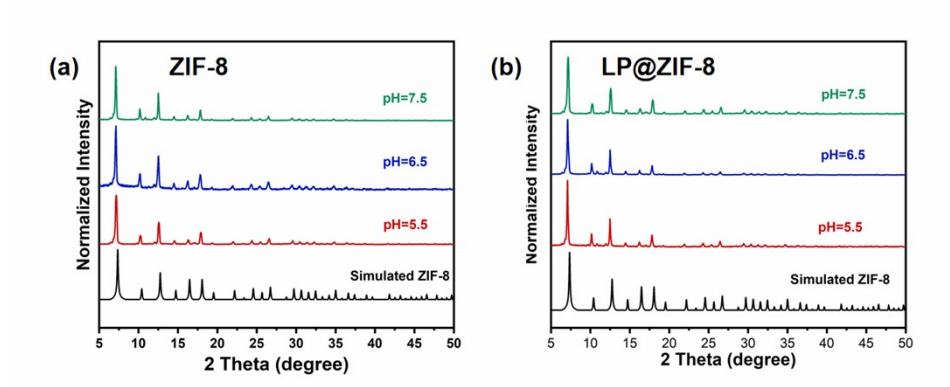

Figure S1. The PXRD pattern of ZIF-8(a) and LP@ZIF-8(b) after treatment in aqueous solutions with different pH values.

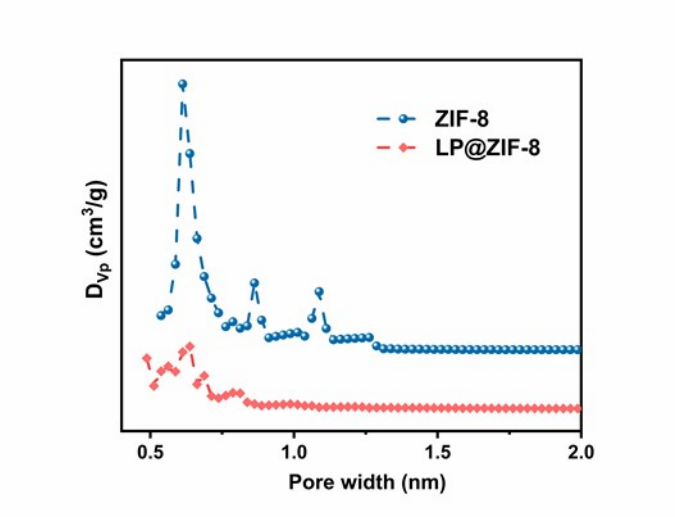

Figure S2. Pore width distribution profiles of ZIF-8, LP@ZIF-8

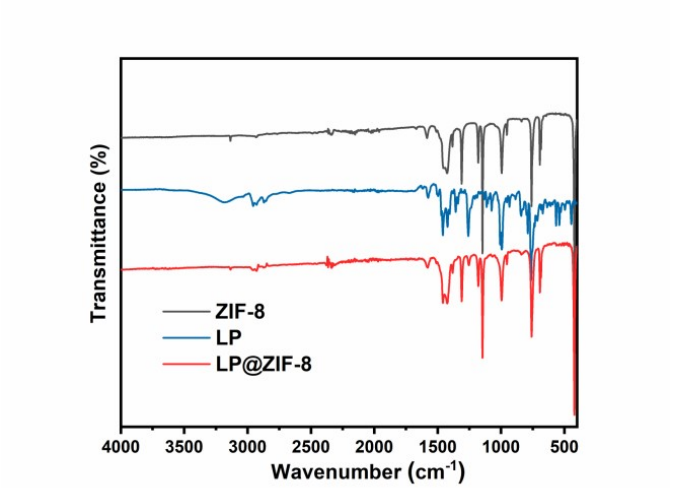

Figure S3. FT-IR spectra of ZIF-8, LP, and LP@ZIF-8

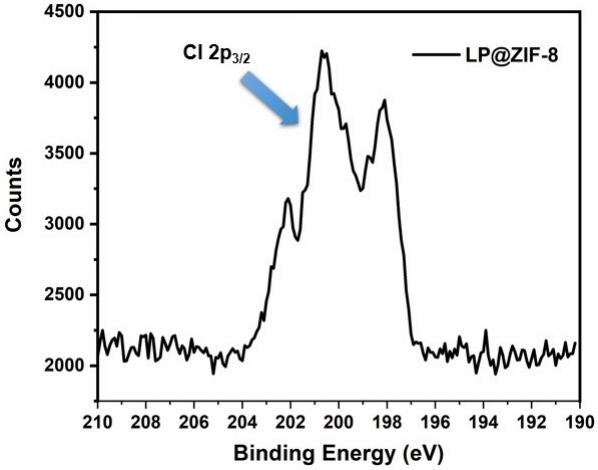

Figure S4. High-resolution XPS spectra of Cl 2p3/2 in LP@ZIF-8.

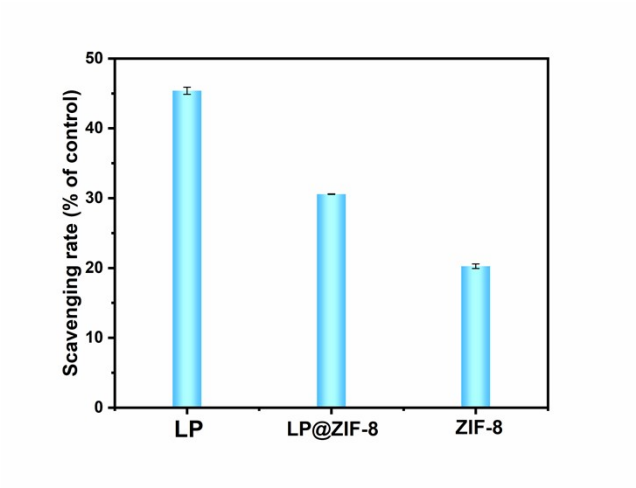

Figure S5. In vitro antioxidant activity of LP, ZIF-8 and LP@ZIF-8 as determined by ABTS free radical scavenging assays. *P < 0.05, **P < 0.01, and ***P < 0.001

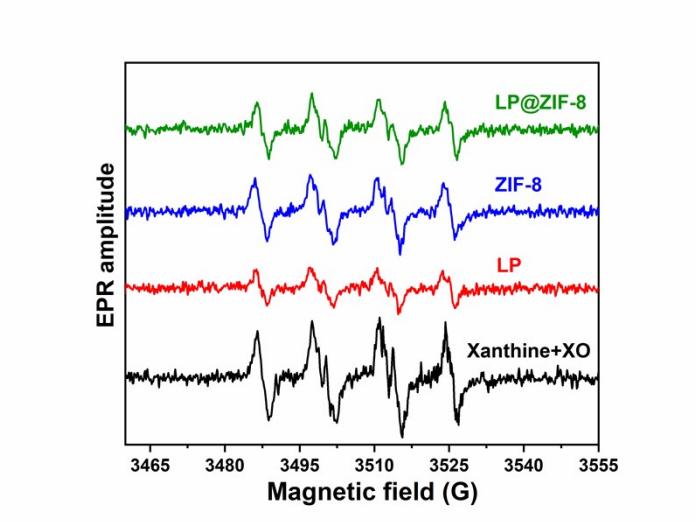

Figure S6. Electron paramagnetic resonance spectra analysis of the $\cdot O_2^-$ scavenging of LP, ZIF-8, and LP@ZIF-8.

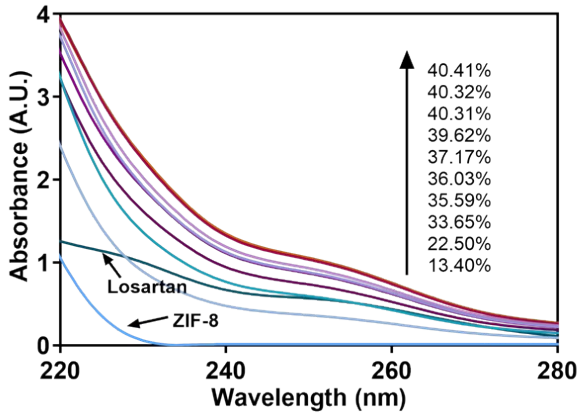

Figure S7. UV-VIS spectra of LP@ZIF-8 with different concentrations of LP

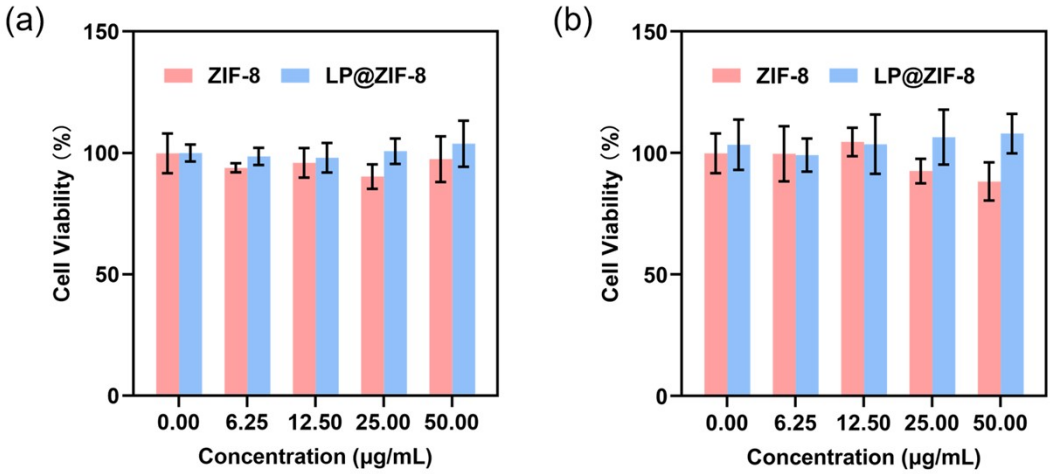

Figure S8. Cell viability of ZIF-8 and LP@ZIF-8 in (a) HUVECs and (b) macrophages. Data are means ± SD (n=4)

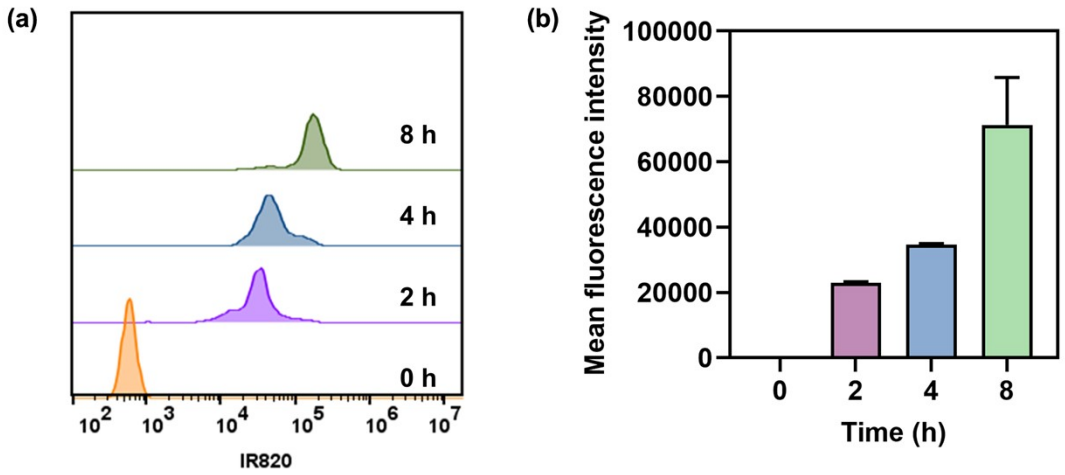

Figure S9. Flow cytometry data for normal macrophages following incubation with IR820@ZIF-8 for 0, 2, 4, and 8 h. (c) FlowJo was used to analyze mean fluorescence intensity (MFI) values for data shown in (b). Data are means ±SD (n = 3).

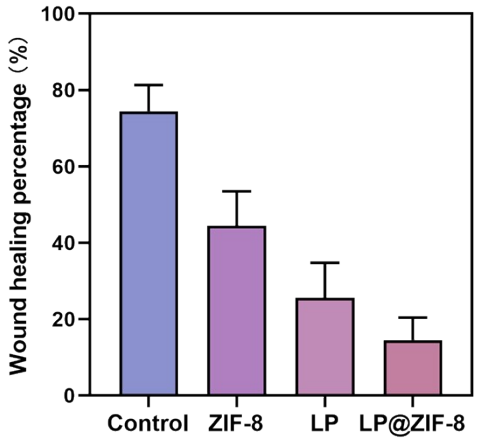

Figure S10. The wound healing percentage of ZIF-8, LP, and LP@ZIF-8 via cell stracting. Data are means ± SD (n = 3).

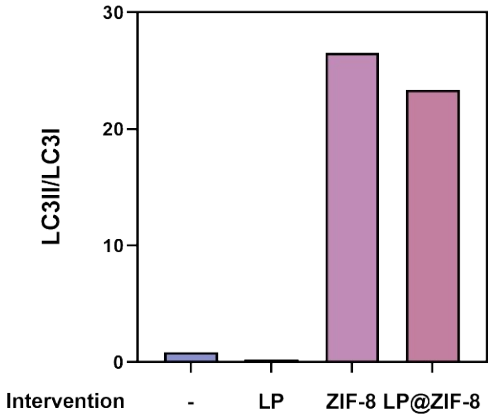

Figure S11. Quantitative detection of the LC3II/LC3I expression level with different interventions in foam cells.

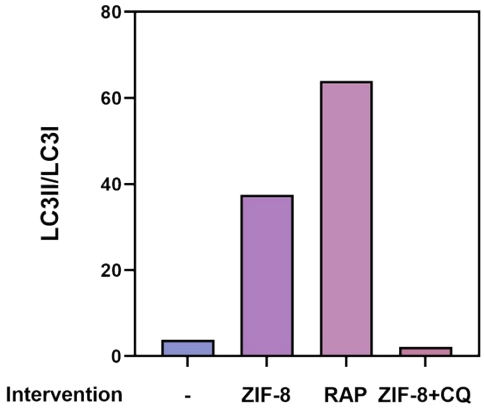

Figure S12. Quantitative detection of the LC3II/LC3I expression level with different interventions in foam cells.

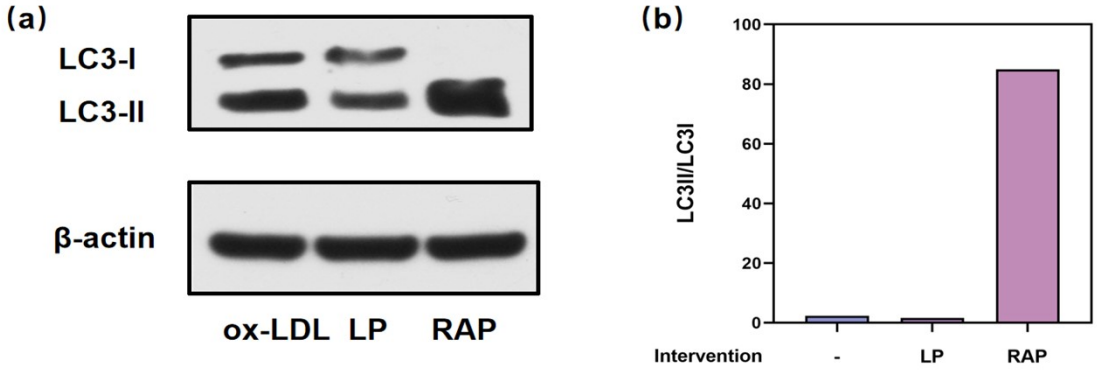

Figure S13. Western blot analysis of the LC3II/LC3I ratio after culture with different interventions (a) qualitatively and (b) quantitatively.

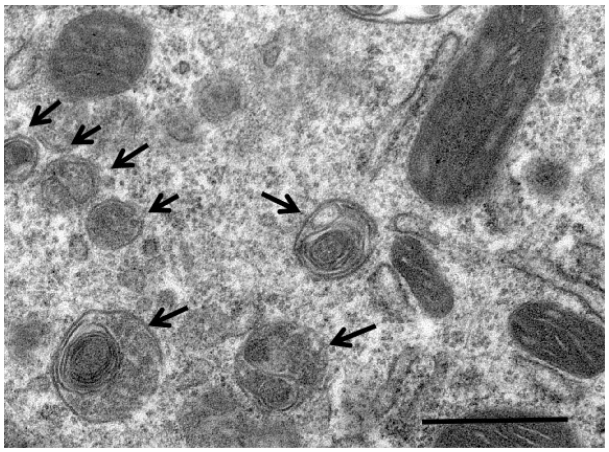

Figure S14. TEM images of autophagosomes in foam cells after treatment with ZIF-8 and. Black arrows were added to outline the double-membrane structures of autophagosomes.Scar bar=500 nm.

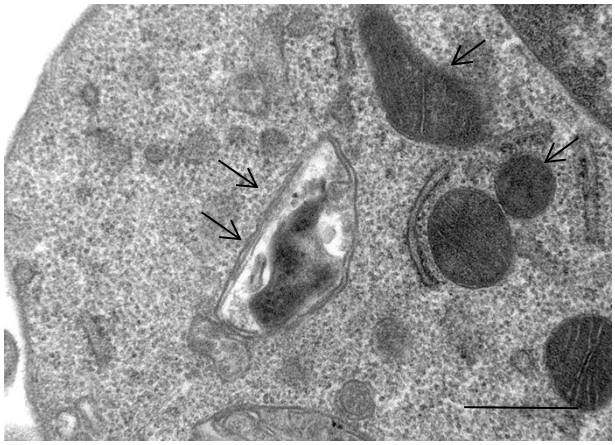

Figure S15. TEM images of autophagosomes in foam cells after treatment with LP@ZIF-8. Black arrows were added to outline the double-membrane structures of autophagosomes.Scar bar=500 nm.

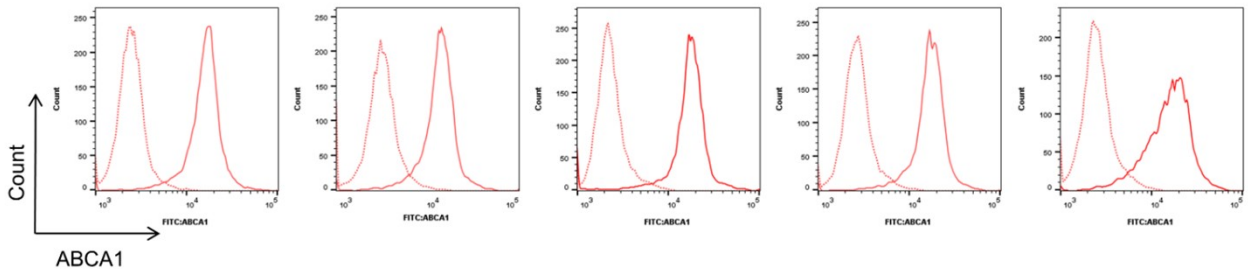

Figure S16. Flow cytometry overlay histogram showing Raw 264.7 cells stained with ABCA1 (red line).

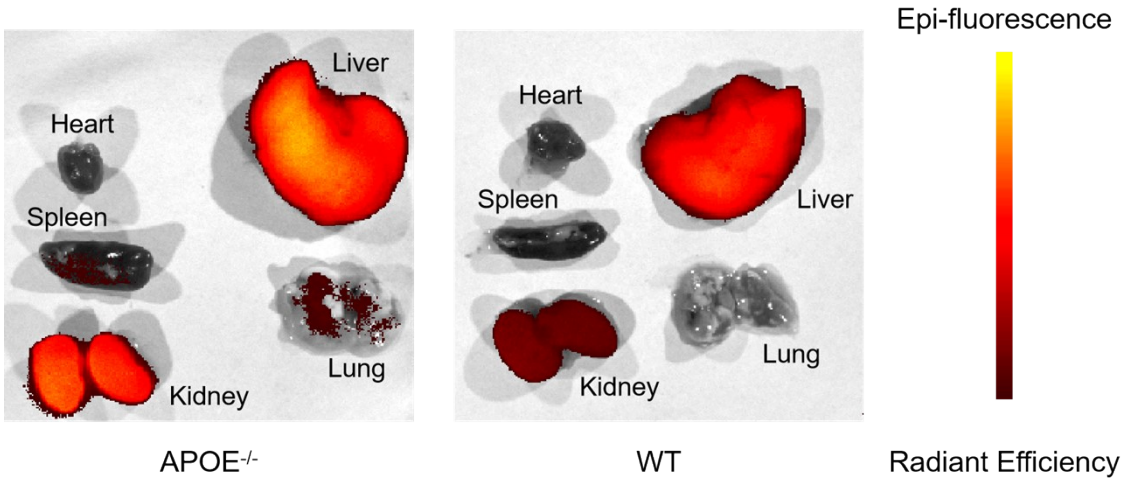

Figure S17. Fluorescence images of the main organs separated from AS mice and healthy controls after 48 h of in vivo imaging

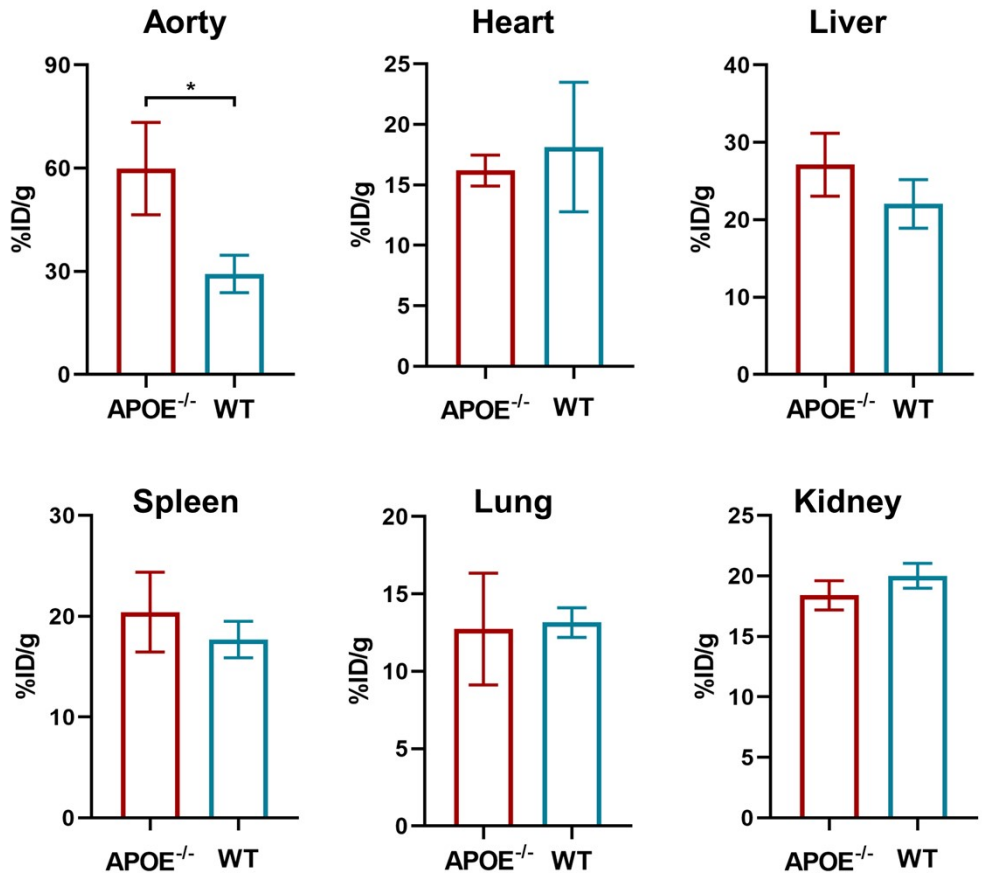

Figure S18. (a) Inductively coupled plasma–mass spectrometry (ICP–MS) of Zn content in the aorta, heart, liver, spleen, lung, and kidney after treatment. (b) Time-concentration curve of zinc in blood from AS mice after a single dose i.v. administration. Data are means ± SD (n = 4).

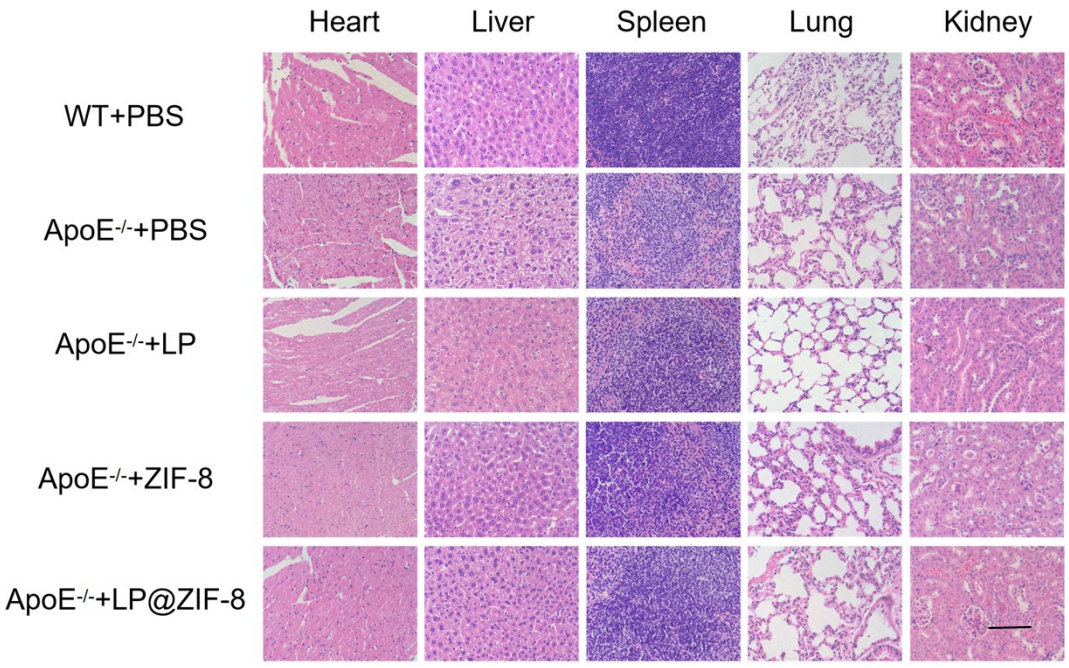

Figure S19. Representative histology (H&E) images of major organs were collected from AS mice with different treatments (PBS; free LP; ZIF-8; and LP@ZIF-8) and healthy control (PBS only) groups of mice after 6 weeks (Scale bar = 100 μm).